

# Ti<sub>3</sub>C<sub>2</sub>T<sub>x</sub> Solid Lubricant Coatings in Rolling Bearings with Remarkable Performance beyond State-of-the-Art Materials

Max Marian<sup>1, a\*</sup>, Klara Feile<sup>1, b</sup>, Benedict Rothhammer<sup>1, c</sup>, Marcel Bartz<sup>1, d</sup>, Sandro Wartzack<sup>1, e</sup>, Armin Seynstahl<sup>2, f</sup>, Stephan Tremmel<sup>2, g</sup>, Sebastian Krauß<sup>3, h</sup>, Benoit Merle<sup>3, i</sup>, Thomas Böhm<sup>4, j</sup>, Bo Wang<sup>5, k</sup>, Brian C. Wyatt<sup>6, l</sup>, Babak Anasori<sup>6, m</sup> and Andreas Rosenkranz<sup>7, n\*</sup>

<sup>1</sup> Engineering Design, Friedrich-Alexander-University Erlangen-Nuremberg (FAU), Erlangen, Germany

<sup>2</sup> Engineering Design and CAD, University of Bayreuth, Bayreuth, Germany

<sup>3</sup> Materials Science & Engineering, Institute I, Interdisciplinary Center for Nanostructured Films (IZNF), Friedrich-Alexander-University Erlangen-Nuremberg (FAU), Erlangen, Germany

<sup>4</sup> Forschungszentrum Jülich GmbH, Helmholtz-Institute Erlangen-Nürnberg for Renewable Energy, Erlangen, Germany

<sup>5</sup> Key Laboratory of Marine New Materials and Related Technology, Zhejiang Key Laboratory of Marine Materials and Protection Technology, Ningbo Institute of Material Technology & Engineering, Chinese Academy of Sciences, Ningbo, People's Republic of China

<sup>6</sup> Department of Mechanical and Energy Engineering, and Integrated Nanosystems Development Institute, Purdue School of Engineering and Technology, Indiana University-Purdue University Indianapolis, USA

<sup>7</sup> Department of Chemical Engineering, Biotechnology and Materials (FCFM), Universidad de Chile, Santiago, Chile

<sup>a</sup> marian@mfk.fau.de, <sup>b</sup> klara.feile@fau.de, <sup>c</sup> rothhammer@mfk.fau.de, <sup>d</sup> bartz@mfk.fau.de, <sup>e</sup> wartzack@mfk.fau.de,

<sup>f</sup> armin.seynstahl@uni-bayreuth.de, <sup>g</sup> stephan.tremmel@uni-bayreuth.de, <sup>h</sup> sebastian.s.krauss@fau.de,

<sup>i</sup> benoit.merle@fau.de, <sup>j</sup> t.boehm@fz-juelich.de, <sup>k</sup> wangb@nimte.ac.cn, <sup>l</sup> bcwyatt@iu.edu, <sup>m</sup> banasori@iupui.edu,

<sup>n</sup> arosenkranz@ing.uchile.cl

\* Corresponding authors

## Abstract

Two-dimensional (2D) transition metal carbides, nitrides, and carbonitrides, known as MXenes, are a growing class of 2D materials, which offer great solid lubrication ability for low friction applications due to their weakly bonded multi-layer structure and tribo-layer formation with self-lubricating characteristics. To date, most studies have assessed their tribological response in basic laboratory tests. However, these tests do not adequately reflect the complex geometries, kinematics, and stresses present in machine components. Here, we aim at bridging this gap through assessment of the friction and wear performance of multi-layer Ti<sub>3</sub>C<sub>2</sub>T<sub>x</sub> MXene solid lubricant coatings used in rolling bearings. MXenes' tribological response is compared with state-of-the-art solid lubricant coatings, which include molybdenum disulfide (MoS<sub>2</sub>), tungsten-doped hydrogenated amorphous carbon (a-C:H:W), and hydrogen-free, more graphite-like amorphous carbon (a-C). Multi-layer Ti<sub>3</sub>C<sub>2</sub>T<sub>x</sub> MXene coatings reduce wear on the bearing washers by up to 94 %, which can be attributed to the transfer of the lubricious MXene nano-sheets to secondary tribo-contacts of the bearing. While the frictional torque of all solid lubricant coatings is similar during steady-operation, the MXene-coated bearings extend the service life by 30 % and 55 % compared to MoS<sub>2</sub> and DLC, respectively. This

---

This is the author's manuscript of the article published in final edited form as:

Marian, M., Feile, K., Rothhammer, B., Bartz, M., Wartzack, S., Seynstahl, A., Tremmel, S., Krauß, S., Merle, B., Böhm, T., Wang, B., Wyatt, B. C., Anasori, B., & Rosenkranz, A. (2021). Ti<sub>3</sub>C<sub>2</sub>T<sub>x</sub> solid lubricant coatings in rolling bearings with remarkable performance beyond state-of-the-art materials. *Applied Materials Today*, 25, 101202. <https://doi.org/10.1016/j.apmt.2021.101202>

36 contribution demonstrates the ability of MXene solid lubricant coatings to outperform state-of-the-art solid  
37 lubricants in dry-running machine components such as rolling bearings.

## 38 **Keywords**

39 2D materials; MXenes; MoS<sub>2</sub>; DLC; solid lubrication; rolling bearings

## 40 **1. Introduction**

41 MXenes, an emerging class of 2D nanomaterials of early transition metal carbides, nitrides, and  
42 carbonitrides, have gained notable attention in the scientific community due to their outstanding  
43 material's performance [1–3]. MXenes are denoted by the general formula of  $M_{n+1}X_nT_x$  ( $n = 1$  to 4),  
44 for which M stands for  $n + 1$  layers of early transition metal from groups 3 - 5 in the  $3d - 5d$  block,  
45 X represents  $n$  layers of carbon, nitrogen, or mixtures of both which interleave the layers of M, and  
46  $T_x$  represents the variety of surface terminations [4]. Compared to graphene and its derivatives,  
47 MXenes exhibit numerous similarities such as their 2D character, strong in-plane bonding  
48 characteristics, and high surface-to-volume ratios [5]. In contrast to other state-of-the-art 2D  
49 nanomaterials, MXenes offer enhanced interlayer interactions, which are not only based on van der  
50 Waals forces, but also include electrostatic and intermolecular interactions due to functional surface  
51 groups [6]. Moreover, MXenes allow for property tuning through the use of different early  
52 transition metals or by adjusting the ratio between carbon and nitrogen, which gives them an  
53 inherent chemical diversity [5,7]. Their structural, chemical and compositional diversity together  
54 with their strong intralayer primary bonding and relatively weaker interlayer secondary bonding  
55 characteristics make MXenes promising 2D nano-materials for mechanical and tribological  
56 applications [5,8].

57 With regards to machine components like rolling bearings, which are representative for highly  
58 stressed and high volume machine elements, solid lubricant coatings are utilized when these  
59 systems cannot be lubricated with conventional oils or greases due to severe environmental  
60 conditions. This comprises very high and low temperatures, vacuum, radiation, or due to strict

61 requirements regarding cleanliness, hygiene, and environmental friendliness [9,10]. In the context  
62 of solid lubricants, soft metals, polymers, transition metal dichalcogenides (TMDs), and carbon-  
63 based materials are frequently used [11]. Thereby, soft metals and/or polymers feature some  
64 limitations particularly in the case of pronounced sliding or at elevated pressures and  
65 temperatures [12,13]. TMDs and in particular molybdenum disulfide ( $\text{MoS}_2$ ) exhibit excellent  
66 sliding properties over a wide range of contact conditions, loads, and temperatures because of their  
67 hexagonal crystal structure and the ease of basal plane slip [14]. Due to the tendency to oxidize  
68 under atmospheric conditions and the significant influence of humidity [15,16], TMDs applications  
69 are mainly in dry and vacuum environments. In this respect,  $\text{MoS}_2$  coatings have also been  
70 successfully employed for rolling bearing components [17,18]. Graphite, graphene, and their  
71 derivatives also offer good solid lubrication properties owing to the easy-to-shear ability of its  
72 densely packed and atomically smooth surface, especially but not limited to moist and ambient  
73 environments [19]. Nevertheless, there are only few application-oriented studies on highly loaded  
74 rolling-sliding contacts as encountered in rolling bearings [20]. In addition, amorphous or diamond-  
75 like carbon (DLC) coatings with high hardness, low wear rates and low friction coefficients are  
76 promising alternatives [21]. These coatings can be doped with metals or lightweight elements to  
77 accommodate relatively large residual compressive stresses and prevent delamination [22], and thus  
78 have found several applications in commercial products. Like other solid lubricants,  
79 their tribological properties exhibit a dependence on the operating conditions and environment,  
80 whereby hydrogen-free DLC coatings perform well in humid air, and hydrogenated coatings  
81 perform better in dry or inert gas environments [11]. Amorphous carbon coatings have also  
82 been successfully applied to highly loaded contacts in rolling element bearings [23–25]. One of the  
83 major advantages of  $\text{MoS}_2$  or DLC coatings is that the components do not have to be  
84 geometrically modified compared to the operation without solid lubricant coatings, since the  
85 involved coating thicknesses do not impair the function.

86 Although these aforementioned materials have been extensively studied in previous publications,  
87 the fundamental tribological behavior of MXenes has recently come into the focus of the  
88 tribological community [5,26,27]. Initially, MXenes were studied as lubricant additives in  
89 paraffin [28], poly-(alpha)-olefin [29], and other base oils [30,31] to optimize the resulting friction  
90 and wear performance. Furthermore, MXenes have been used in metal [32,33] and polymer [34,35]  
91 matrix composites as the reinforcement phase. In particular, the use of MXenes as solid lubricant  
92 coatings demonstrated promising results at the nano- and macroscopic scales for enhancing friction  
93 and wear behavior [36–40]. Besides the fundamental dependencies of friction and wear on contact  
94 pressure and relative humidity [41], the solid lubrication ability of hybrid coatings (combination of  
95 MXenes and graphene/graphene oxide or MXenes and nanodiamonds) has been investigated [42–  
96 44]. Very recently, 100-nm-thick multi-layer MXene coatings deposited by electro-spraying onto  
97 stainless steel have verified their outstanding wear resistance and ability to outperform state-of-the-  
98 art 2D materials with regard to their durability and longevity [45]. The improved wear performance  
99 was traced back to the formation of a beneficial tribo-layer consisting of amorphous and  
100 nanocrystalline iron oxide intermixed with thermally and structurally degraded MXenes. This  
101 observation aligns well with the good wear performance of hybrid MXene coatings.

102 Until now, the tribological studies on MXenes have mainly focused on titanium-based MXenes  
103 (mainly  $Ti_3C_2T_x$  nano-sheets), and the fundamental effects/mechanisms were explored by laboratory  
104 model tests under pure sliding motion. When this knowledge is transferred to macro-scale and  
105 application-oriented conditions with more complex geometries, kinematics and stresses,  
106 the underlying mechanisms are yet to be explored [46]. Recently, Marian *et al.* [47] applied  
107 MXene nano-sheets as solid lubricants to highly loaded rolling-sliding contacts of machine  
108 elements. In component level testing, an up to 3.2-fold friction reduction, a decrease in the  
109 cumulative linear wear by 2.9 times, and an extension of service life by a factor of 2.1 were  
110 observed for  $Ti_3C_2T_x$ -coated thrust ball bearings, compared to uncoated references. This  
111 indicates the potential of MXenes to lubricate dry-running machine elements effectively and  
efficiently.

112 Although various solid lubricant coating systems with specific advantages and limitations have been  
113 used for dry-running machine components, the development and qualification of novel MXenes as  
114 solid lubricant coatings with comparison to other state-of-the art 2D materials is currently scarce.  
115 Apart from our own previous study [47], MXenes' tribological performance has been mainly  
116 assessed by fundamental laboratory tests using simplified test rigs, which do not adequately  
117 represent the conditions of highly loaded sliding-rolling contacts and the interaction of multiple  
118 components in machine elements such as rolling bearings. This study aims at elucidating the  
119 friction and wear performance of multi-layer  $Ti_3C_2T_x$  solid lubricant coatings in rolling bearings  
120 working under realistic conditions. The tribological performance of the MXene coatings is  
121 compared with the performance of state-of-the art solid lubricant coatings, namely DLC and  $MoS_2$ .

## 122 **2. Materials and Methods**

### 123 ***2.1. Specimens***

124 Due to the large sliding and spinning friction portions as well as the facilitated possibility for  
125 coating deposition, commercially available 51201 thrust ball bearing washers specified in  
126 ISO 104 [48] were used. The complete axial rolling bearing consisted of shaft washer, ball cage  
127 assembly (rolling elements + sheet metal cage) and housing washer. The rolling elements as well as  
128 the bearing washers were made of 100Cr6 (1.3505, AISI 52100) bearing steel.

### 129 ***2.2. Coating deposition***

130 To evaluate their solid lubrication ability,  $Ti_3C_2T_x$ ,  $MoS_2$  and two DLC coatings were deposited on  
131 the bearing washer raceways. Prior to deposition, the bearing components were ultrasonically  
132 cleaned in acetone and isopropyl alcohol for 10 minutes each (Sonorex Super RK 255H 160 W  
133 35 Hz, Bandelin electronic GmbH & Co. KG, Berlin, Germany) and subsequently blow-dried with  
134 nitrogen.

### 135 2.2.1. $Ti_3C_2T_x$ coating

136 The synthesis of multi-layer  $Ti_3C_2T_x$  nano-sheets made use of 10 g of  $Ti_3AlC_2$  powder (Forsman  
137 Scientific Co. Ltd., Beijing, China), which was immersed in 100 mL of a 40 % HF solution. The  
138 solution was stirred at room temperature for about one day prior to a washing and centrifugation  
139 treatment. After one centrifugation step, the supernatant was poured out and fresh deionized water  
140 was added, until reaching a pH of about 6. Subsequently, the final MXenes were filtered under  
141 vacuum and freeze-dried at a temperature of  $-60\text{ }^\circ\text{C}$  and pressure of below 30 Pa for 24 hours. The  
142 MXenes were then dispersed in acetone (10 mg/mL), stirred (AREX-6 digital heating magnetic  
143 stirrer, Velp Scientifica Srl, Usmate, Italy) and ultrasonicated (Sonorex Super RK 255H, 160 W,  
144 35 Hz, Bandelin electronic GmbH & Co. KG, Berlin, Germany) at room temperature for 10 minutes  
145 each to ensure good dispersion. Prior to testing, 300  $\mu\text{L}$  of the dispersion were drop-casted (1000  
146 series gastight 81420, Hamilton Germany GmbH, Gräfelfing, Germany) onto each bearing washer  
147 raceway, which yielded the  $Ti_3C_2T_x$  coating after solvent evaporation. In contrast to previous  
148 studies [47], no MXenes were applied to the ball cage assembly to ensure better comparability with  
149 the  $MoS_2$ - and DLC-coated bearings.

### 150 2.2.2. DLC coatings

151 The DLC coatings were fabricated using an industrial-scale coating plant (TT 300 K4, H-O-T Härte  
152 und Oberflächentechnik GmbH & Co. KG, Nuremberg, Germany) for physical vapor deposition  
153 (PVD). Two coating systems with tungsten-containing, hydrogenated amorphous carbon (a-C:H:W)  
154 and hydrogen-free amorphous carbon (a-C) as tribologically effective functional layers were  
155 deposited under 2-fold rotation. These were selected due to their promising tribological behavior  
156 under dry conditions [49,50] and in rolling bearings [23,24,51]. The chamber was initially  
157 evacuated to a base pressure of  $2.4 \times 10^{-4}$  Pa and heated to  $250\text{ }^\circ\text{C}$  for 40 minutes. Subsequently, the  
158 samples were argon-ion ( $Ar^+$ ) plasma etched for 40 minutes using an argon (Ar) flow of 500 sccm  
159 and a bipolar pulsed bias voltage of  $-500\text{ V}$  (pulse frequency 40 kHz, reverse recovery time 5  $\mu\text{s}$ ).

160 The same cleaning procedure was carried out for the powder metallurgical chromium (Cr, purity  
 161 99.998 %), tungsten carbide (WC, purity 99.9 %), and graphite (C, purity 99.998 %) targets  
 162 ( $267.5 \times 170$  mm). First, a thin Cr adhesion layer was applied and transferred to a WC support  
 163 layer. Efforts were made to achieve graded transitions to the substrate and between the individual  
 164 layers by continuously adjusting the process parameters (please refer to Table 1). The a-C:H:W and  
 165 a-C layers were subsequently deposited by reactive and non-reactive PVD through unbalanced  
 166 magnetron UBM sputtering under argon-acetylene ( $\text{Ar-C}_2\text{H}_2$ ) and pure Ar atmosphere, respectively.  
 167 In contrast to the a-C:H:W layer, the a-C layer had to be applied in two steps. The first step was to  
 168 lower the tungsten and hydrogen content by gradually reducing the cathode power and reducing the  
 169  $\text{C}_2\text{H}_2$  flow (purity 99.5 %). Secondly, the coating process was interrupted to replace the Cr with the  
 170 C target due to the coating plant configuration. Subsequently, the chamber was re-evacuated and  
 171 heated to  $100^\circ\text{C}$  for 40 minutes, followed by  $\text{Ar}^+$ -ion plasma etching for 5 minutes. Thereafter, the  
 172 a-C functional layer was deposited with a gradual increase in bias voltage.

173 **Table 1.** Cathode, process and reactive gas parameters for the deposition of the a-C:H:W, a-C, and  
 174  $\text{MoS}_2$  coatings. The dashed line indicates the interruption in the deposition process.

coating	layer	power	pulse frequency	reverse recovery time	duration	bias voltage	chamber temperature	Ar flow	$\text{C}_2\text{H}_2$ flow
a-C:H:W	Cr	5.0 kW	40 kHz	5 $\mu\text{s}$	240 s	-100 V	$160^\circ\text{C}$	180 sccm	-
	CrWC	5.0   0.3 $\nearrow$ 1.2 kW	40 kHz	5 $\mu\text{s}$	960 s	-100 V	$150^\circ\text{C}$	180 sccm	-
	WC	1.2 kW	40 kHz	5 $\mu\text{s}$	1080 s	-100 V	$130^\circ\text{C}$	195 sccm	-
	a-C:H:W	1.5 kW	40 kHz	5 $\mu\text{s}$	5400 s	0 V	$100^\circ\text{C}$	90 sccm	25 sccm
a-C	Cr	5.0 kW	40 kHz	5 $\mu\text{s}$	240 s	-100 V	$160^\circ\text{C}$	180 sccm	-
	CrWC	5.0   0.3 $\nearrow$ 1.2 kW	40 kHz	5 $\mu\text{s}$	960 s	-100 V	$150^\circ\text{C}$	180 sccm	-
	WC	1.2 kW	40 kHz	5 $\mu\text{s}$	1080 s	-100 V	$130^\circ\text{C}$	195 sccm	-
	a-C:H:W	1.5 kW	40 kHz	5 $\mu\text{s}$	5400 s	-50 V	$100^\circ\text{C}$	90 sccm	25 sccm
	a-C	2.0 kW	75 kHz	3 $\mu\text{s}$	7205 s	-30 $\nearrow$ -170 V	$100^\circ\text{C}$	90 sccm	-
$\text{MoS}_2$	$\text{MoS}_2$	2.0 kW	70 kHz	4 $\mu\text{s}$	7200 s	0 V	$50^\circ\text{C}$	120 sccm	-

### 175 2.2.3. $\text{MoS}_2$ coating

176 Under 3-fold rotation, the substrates were  $\text{MoS}_2$ -coated using the same coating plant as for DLC  
 177 and a hot-pressed powder target (purity 99.5 %,  $260 \times 163$  mm). Prior to deposition, the chamber

178 was evacuated to achieve an initial pressure of  $2.5 \times 10^{-3}$  Pa and was heated to 50 °C. Subsequently,  
179 the specimens' surfaces were cleaned and activated by Ar<sup>+</sup>-ion plasma etching with the same  
180 procedure as described in section 2.2. Furthermore, cathode sputtering was performed for 3 minutes  
181 with closed shutters to remove impurities and the thin oxide layer from the target. Afterwards, the  
182 MoS<sub>2</sub> coating was deposited by PVD through UBM sputtering under Ar atmosphere without  
183 applying any additional adhesion layer. The deposition parameters were selected based  
184 upon [16,52,53] and are summarized in Table 1.

### 185 **2.3. Coating characterization**

186 The thickness and structure of the as-deposited coatings were characterized utilizing a focused ion  
187 beam scanning electron microscope (FIB-SEM; NanoLab 600i, FEI Thermo Fisher, Hillsboro, OR,  
188 USA). For electron imaging, secondary electron contrast, an acceleration voltage of 5 kV, an  
189 electron current of 0.69 nA, and a working distance of 4 mm were used. Cross-sections of the  
190 coatings were fabricated by FIB milling. At first, a protective platinum (Pt) layer was locally  
191 deposited onto the samples to avoid FIB damage [54]. Decreasing ion beam currents of 2.5, 0.79,  
192 and 0.23 nA were subsequently used for sequentially milling the coatings. After final ion polishing,  
193 the cross sections were investigated by SEM with a tilting angle of 52°. Furthermore, the  
194 stoichiometry of the MoS<sub>2</sub> coating was investigated via energy-dispersive X-ray spectroscopy  
195 (EDX; Oxford Instruments plc, Abingdon, UK) using an acceleration voltage of 20 kV and an  
196 electron current of 2.7 nA. The spectra were recorded while scanning an area of approx.  
197  $10 \times 6 \mu\text{m}^2$ . In addition, EDX line scans in the FIB-milled cross sections were recorded to reveal  
198 the coatings' architectures. Moreover, digital light microscopic images and Raman spectra were  
199 acquired (WITec alpha 300R, WITec Wissenschaftliche Instrumente und Technologie GmbH, Ulm,  
200 Germany) with excitation at 457 nm and a laser power of 0.15 mW. The spectra were integrated for  
201 5 s with 5 accumulations and background-corrected (shape-based algorithm, WITec Project  
202 FIVE+). Finally, averaged spectra from different spots on the samples were obtained after intensity  
203 normalization.



## 204 **2.4. Tribological testing**

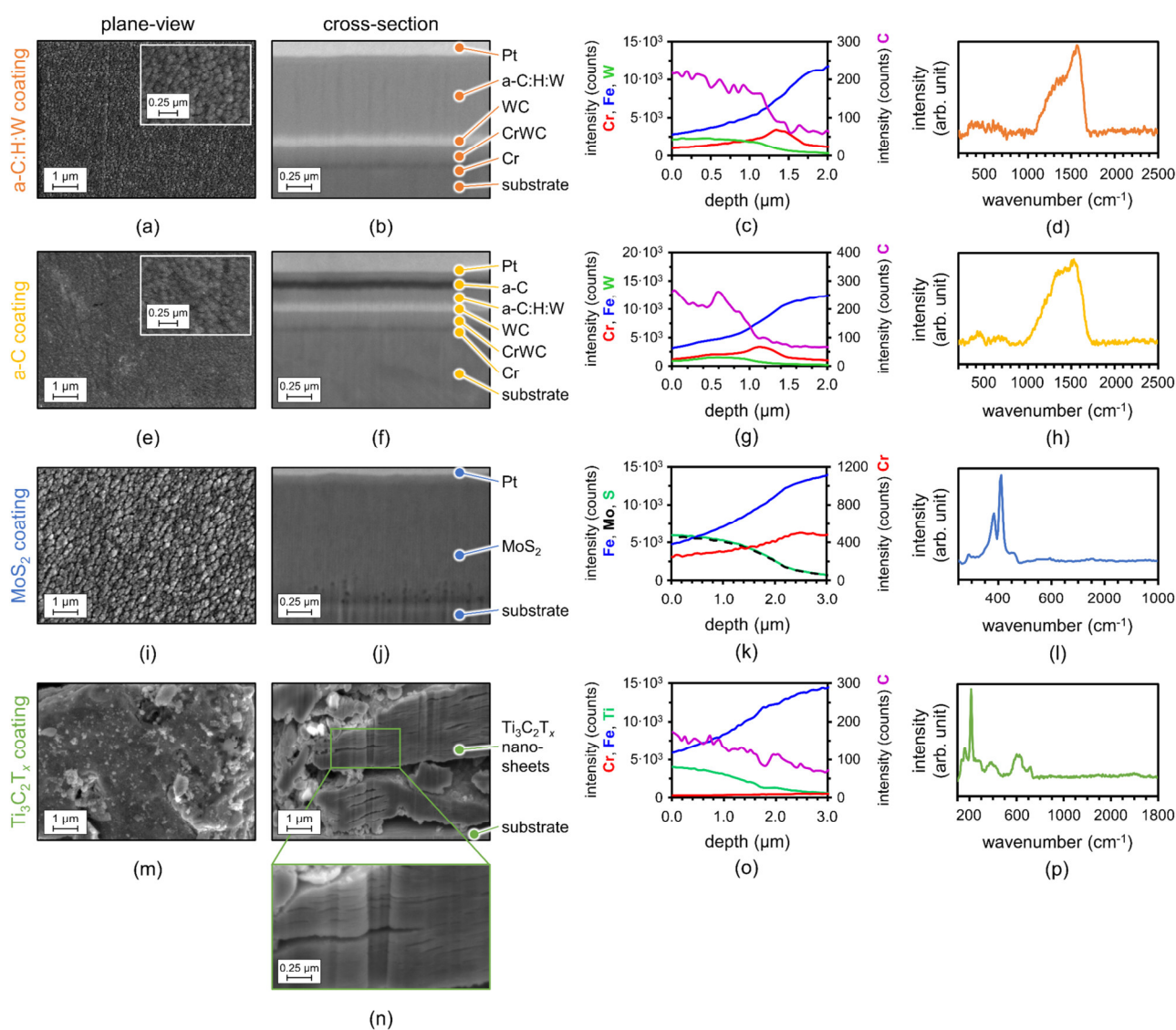
205 Tribological tests were performed on a TRM1000 tribometer (Wazau Mess- + Prüfsysteme GmbH,  
206 Berlin, Germany) with modified set-up under laboratory ambient conditions [47]. Thereby, the  
207 housing washer was driven with  $1000 \text{ min}^{-1}$  (10 % of the catalog speed limit), while the shaft  
208 washer was fixed and cardanically mounted for uniform loading. A normal force of 130 N (15 % of  
209 the catalog axial fatigue limiting load) was applied via weights on the stationary mounting,  
210 providing an initial Hertzian pressure of 800 MPa. The measurements, especially the resulting  
211 frictional torque, were recorded at a frequency of 10 Hz. Similar to [47], a frictional torque of  
212 1.3 Nm was defined as termination criterion of the tests. Three experiments were performed for  
213 each bearing type (uncoated references, a-C:H:W-, a-C-, MoS<sub>2</sub>- and MXene-coated) with new  
214 samples. The measurements were analyzed for a distinct rise in the frictional torque, which  
215 indicated incipient coating failure, thus defining the end of the service life. Since each volume  
216 element on the bearing washers is rolled over several times per revolution, the number of endured  
217 overrollings was used as a criterion for comparison. Additionally, the frictional torque during  
218 service life and the gravimetric wear were analyzed. Regarding the latter, the bearings were  
219 weighed prior to and after tribological testing (ALS-A/ALJ-A, Kern & Sohn GmbH, Balingen-  
220 Frommern, Germany).

## 221 **3. Results and Discussion**

### 222 ***3.1. Coating properties***

223 SEM micrographs of the as-deposited coatings (plane-view and FIB-milled cross-sections), averaged  
224 EDX line scans and the averaged Raman spectra are depicted in Figure 1. The thicknesses of the a-  
225 C:H:W and the a-C coatings were measured to be around 1.5 and 1.0  $\mu\text{m}$ , respectively (Figure 1b, f).  
226 The multilayer character with the WC inter- and the Cr adhesion layers can also be seen from the  
227 EDX line scans (Figure 1c, g). The cauliflower-like topographies of both coatings pointed towards a  
228 DLC-typical and fine columnar growth [55] (Figure 1a, e). The Raman spectra

229 (Figure 1d, h) featured two distinct peaks around 1340 and 1555  $\text{cm}^{-1}$ , which are characteristic for  
 230 the D- and G-bands of DLC coatings [56,57]. For the a-C:H:W coating (Figure 1d), the ratio  
 231 between the peak intensities of the D- and G-bands, which is an indicator for the  $\text{sp}^2$  and  $\text{sp}^3$   
 232 content [58], aligns well with hydrogenated amorphous carbon [56]. The spectrum of the a-C  
 233 coating (Figure 1h) suggested a more graphite-like carbon (GLC) [50,59]. Detailed insights in the  
 234 mechanical and chemical characterization of similar coatings can be found elsewhere [49,50].



235

236 **Figure 1.** SEM-micrographs and FIB cross-sections of the as-deposited (a, b) a-C:H:W, (e, f) a-C,  
 237 (i, j) MoS<sub>2</sub> and (m, n) Ti<sub>3</sub>C<sub>2</sub>T<sub>x</sub> coatings. Pt corresponds to a protection layer deposited during FIB  
 238 processing. Averaged EDX line scans of the as-deposited (c) a-C:H:W, (g) a-C, (k) MoS<sub>2</sub> and (o)  
 239 Ti<sub>3</sub>C<sub>2</sub>T<sub>x</sub> coatings. Averaged Raman spectra of the as-deposited (d) a-C:H:W, (h) a-C, (l) MoS<sub>2</sub> and  
 240 (p) Ti<sub>3</sub>C<sub>2</sub>T<sub>x</sub> coatings.

241 The MoS<sub>2</sub> coating featured a thickness of about 1.3 μm, was slightly deficient in sulfur with a S/Mo-  
242 ratio of about 1.82 according to EDX analysis (Figure 1k), and showed a dendritic and porous  
243 growth (Figure 1i, j). This could be attributed to the 3-fold substrate rotation during deposition [52].  
244 The Raman spectrum of the MoS<sub>2</sub> sample (Figure 1l) showed pronounced double peaks at 380 and  
245 407 cm<sup>-1</sup>, which can be attributed to first order E<sub>2g</sub><sup>1</sup> and A<sub>1g</sub> modes of hexagonal MoS<sub>2</sub> [60–64].  
246 Further peaks were observed at 286 and 453 cm<sup>-1</sup>, corresponding to E<sub>1g</sub> and 2LA(M) modes  
247 [60,61,65,66]. A more detailed characterization of similar MoS<sub>2</sub> coatings can be found in [52].

248 The MXene coating mainly consisted of multi-layered Ti<sub>3</sub>C<sub>2</sub>T<sub>x</sub> nano-sheets (Figure 1m, o), for  
249 which the well-known accordion-like structure was observed in the cross-section images  
250 (Figure 1n) [41]. The Raman spectrum (Figure 1p) indicated distinct peaks around 160, 220, and  
251 707 cm<sup>-1</sup> as well as wider peaks around 285, 375, and 600 cm<sup>-1</sup>. The first peak may be correlated  
252 with in-plane Ti<sub>3</sub>C<sub>2</sub>T<sub>x</sub> vibrations or minor contributions originating from anatase TiO<sub>2</sub>, which may  
253 be correlated with smaller particles observed in SEM (bright submicron particles in Figure 1m) and  
254 minor surface oxidation. However, these particles are expected to play a minor role for the  
255 tribological experiments. All other peaks can clearly be assigned to vibrations originating from  
256 Ti<sub>3</sub>C<sub>2</sub>O<sub>2</sub>, Ti<sub>3</sub>C<sub>2</sub>F<sub>2</sub> and Ti<sub>3</sub>C<sub>2</sub>(OH)<sub>2</sub> [67–70]. The occurrence of -O, -F and -(OH) groups can be  
257 explained by the MXenes' synthesis involving selective etching with HF and the replacement of  
258 aluminum with respective surface terminations [41,47]. For a more in-depth characterization of the  
259 MXene coating by high-resolution transmission electron microscopy, X-Ray photoelectron  
260 spectroscopy, or X-Ray diffraction, the interested reader is referred to our previous studies [37,40–  
261 42,47].

262 The MXene layer thickness could be estimated to be between 2 and 4 μm with thickness deviations  
263 over the raceway, which can be traced back to the size of the stacked MXenes as well as the solvent  
264 evaporation during drop-casting, and the raceway's curvature. This resulted in the layer thickness at  
265 the inner and outer edge of the raceway being slightly thinner than the thickness in the center. Due

266

267 to the variation in thicknesses and the less dense character of the  $\text{Ti}_3\text{C}_2\text{T}_x$  coating compared to the  
268  $\text{MoS}_2$  and DLC coatings, a comparison of the usable lubricant volume purely based on the coating  
269 thickness may not be conclusive. The estimation of the available solid lubricant mass allows for a  
270 fairer comparison. In case of the MXene coating, the mass can be estimated based on the known  
271 drop-casting conditions (300  $\mu\text{L}$  at a concentration of 10 mg/mL). For the  $\text{MoS}_2$  and DLC coatings,  
272 the available masses can be approximated based on the raceway geometry of the 51201 thrust ball  
273 bearing washers [48] ( $\sim 4.5 \text{ cm}^2$ ), the measured thickness, and density data from literature  
274 ( $5.1 \text{ g/cm}^3$  for  $\text{MoS}_2$  and  $2.6 \text{ g/cm}^3$  for DLC) [14,71–73]. The estimated available masses for  
275 MXene and  $\text{MoS}_2$  coatings are comparable with about 3 mg, while a-C:H:W and a-C were at about  
276 half of that (1.6 mg for a-C:H:W and 1.1 mg for a-C).

### 277 3.2. Friction, wear, and service life

278 Representative evolutions of the frictional torque versus overrollings are presented in Figure 2 for  
279 the uncoated reference (Figure 2a) as well as the a-C:H:W-, a-C-,  $\text{MoS}_2$ -, and MXene-coated  
280 bearings (Figure 2b-e). All tested specimens initially exhibited a rather low and constant frictional  
281 torque. After a certain test duration, it increased sharply and leveled off with pronounced  
282 fluctuations. Ultimately, it reached the switch-off threshold due to severe cage failure as well as  
283 clamping, fretting, and overheating of the rolling elements, which we considered to be catastrophic  
284 failure [47]. We defined the first pronounced increase in friction exceeding 0.5 Nm as the end of  
285 service life. This corresponds to the end of the bearing's usability due to high friction, non-smooth  
286 operation and incipient wear. The mean number of overrollings as well as the frictional torque until  
287 the end of the service life were compared in Figure 2f, g and Table 2 for the different coating types.  
288 Moreover, the mean gravimetric wear loss after tribological testing is summarized in Table 2 and  
289 depicted in Figure 2 for (h) the shaft and (i) the housing washer as well as (j) the ball cage  
290 assembly. Since the total running time of each individual bearing was different, these values were  
291 normalized to the number of overrollings to enable a fair comparison. Digital optical light  
292 microscopic images of worn surfaces of the MXene-coated washer raceway (a), the corresponding

293 ball (b) and cage (c) with measurement positions for Raman spectroscopy as well as averaged  
 294 spectra (d) are displayed in Figure 3.

295

296

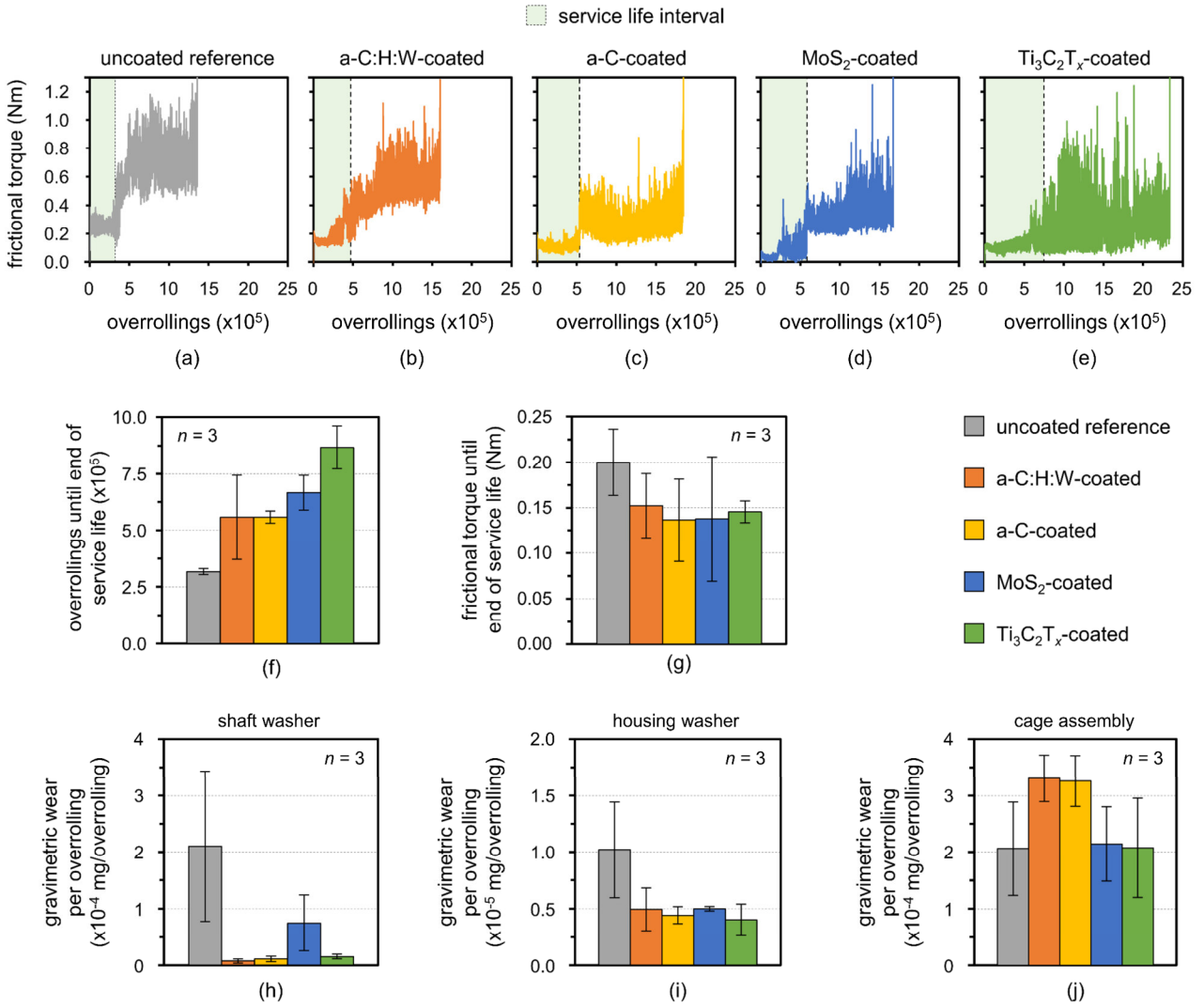
297

298

299 **Table 2.** Averaged number of overrollings and frictional torque until end of service life as well  
 300 as averaged gravimetric wear per overrolling of the shaft washer, housing washer, and ball  
 301 cage assembly, respectively.

	<b>uncoated reference</b>	<b>a-C:H:W</b>	<b>a-C</b>	<b>MoS<sub>2</sub></b>	<b>Ti<sub>3</sub>C<sub>2</sub>T<sub>x</sub></b>
averaged overrollings until end of service life	3.17 x 10 <sup>5</sup>	5.58 x 10 <sup>5</sup>	5.58 x 10 <sup>5</sup>	6.66 x 10 <sup>5</sup>	8.67 x 10 <sup>5</sup>
averaged frictional torque until end of service life	0.20 Nm	0,15 Nm	0,14 Nm	0,14 Nm	0,15 Nm
averaged gravimetric shaft washer wear per overrolling	2.1 x 10 <sup>-4</sup>	7.5 x 10 <sup>-6</sup>	1.1 x 10 <sup>-5</sup>	7.5 x 10 <sup>-5</sup>	1.5 x 10 <sup>-5</sup>
averaged gravimetric housing washer wear per overrolling	1.0 x 10 <sup>-5</sup>	4.9 x 10 <sup>-6</sup>	4.4 x 10 <sup>-6</sup>	5.0 x 10 <sup>-6</sup>	4.0 x 10 <sup>-6</sup>
averaged gravimetric cage assembly wear per overrolling	2.1 x 10 <sup>-4</sup>	3.3 x 10 <sup>-4</sup>	3.3 x 10 <sup>-4</sup>	2.1 x 10 <sup>-4</sup>	2.1 x 10 <sup>-4</sup>

302



303

304 **Figure 2.** Frictional torque versus overrollings for representative tests with (a) uncoated reference,  
 305 (b) a-C:H:W-, (c) a-C-, (d) MoS<sub>2</sub>- and (e) Ti<sub>3</sub>C<sub>2</sub>T<sub>x</sub>-coated bearings (representative graphs). The  
 306 service life interval is indicated by the dashed line and the area highlighted in light green. (f)  
 307 Averaged number of overrollings and (g) averaged frictional torque until end of service life.  
 308 Averaged gravimetric wear per overrolling of (h) shaft washer, (i) housing washer and (j)  
 309 cage assembly. Data show mean  $\pm$  standard deviation for  $n = 3$ .

310 The uncoated reference (Figure 2a) started with the largest frictional torque around 0.2 Nm  
 311 (Table 2, Figure 2g, grey) and its service live ended comparatively early after an average of  
 312  $3.2 \times 10^5$  overrollings (Table 2, Figure 2f, grey). This was due to the lack of a damping lubricant  
 313 and the associated orbital and tilting movements of the ball guided cage with substantial stresses  
 314 building up between the rolling elements and the cage pockets [47]. Accordingly, the frictional  
 315 torque became increasingly unstable, reaching values between 0.6 and 1.1 Nm (Figure 2a) until  
 316 catastrophic failure occurred. Thereby, the bearing washers also showed considerable signs of wear,

317 which was also reflected by the comparatively high gravimetric loss of mass (Table 2, Figure 2h  
318 and i, grey).

319 Bearings coated with solid lubricants demonstrated a slightly lower initial friction level (Figure 2b-  
320 e), which were between 0.13 and 0.15 Nm on average (Table 2, Figure 2g), without significant  
321 differences between the various coating types when taking into account the standard deviations. All  
322 coatings at least ~ doubled the service life of the bearings compared to the uncoated reference  
323 (Table 2, Figure 2f). The bearings also failed due to the fatal cage assembly malfunction, making  
324 reliable statements regarding gravimetric cage wear (Figure 2j) difficult. However, it could be  
325 observed that the wear on the bearing washers was notably reduced by the solid lubricant coatings  
326 (Table 2, Figure 2h and i).

327 The DLC-coated bearings initially showed low frictional torque, which increased to values between  
328 0.4 and 0.8 Nm (a-C:H:W, Figure 2b) as well as 0.15 and 0.6 Nm (a-C, Figure 2c) after the end of  
329 service life. The latter was reached after an average of  $5.6 \times 10^5$  overrollings for both types,  
330 representing a 1.8-fold increase compared to the reference (Table 2, Figure 2f, orange and yellow).  
331 Regarding wear, a significant wear reduction of about 95 % (shaft washer) and 52 % (housing  
332 washer) was verified for both DLC coatings (Table 2, Figure 2h and i, orange and yellow).

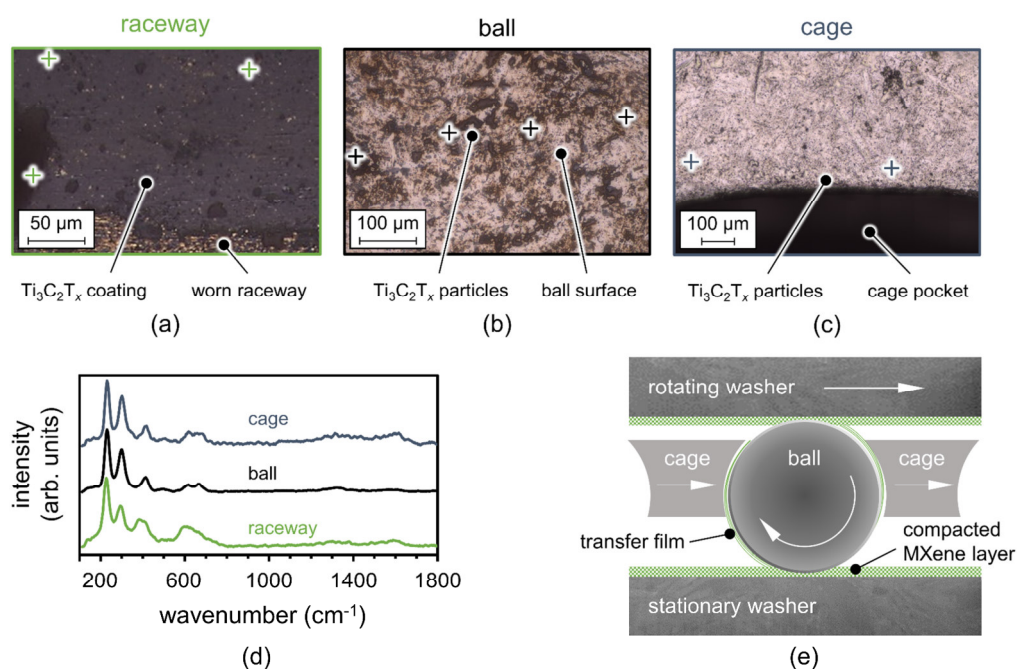
333 In the case of the MoS<sub>2</sub> coating, there was a rise in frictional torque on average after  
334  $6.7 \times 10^5$  overrollings (end of service life), which represented an enhancement by a factor of 2.1  
335 compared to the uncoated reference (Table 2, Figure 2f, blue). This was comparable to previous  
336 results from Vierneusel [74] on undoped and superior to Ti- or Cr-doped MoS<sub>2</sub> coatings with the  
337 same tribometer and setup. Afterwards, the bearings still operated at frictional torque levels  
338 between 0.2 and 0.6 Nm for some time with stronger fluctuations prior to catastrophic failure  
339 (Figure 2d). In terms of wear of the bearing washers, there was a reduction of 64 % (shaft washer)  
340 and 51 % (housing washer) compared to the uncoated reference (Table 2, Figure 2h and i, blue).

341 MXene-coated bearings initially operated at low friction levels, which gradually began to fluctuate  
342 more as the service life approached its end but remained at relatively low levels between 0.1 and

343 0.6 Nm (Figure 2e). The mean service life of  $8.7 \times 10^5$  overrollings exceeded that of the reference  
344 by a factor of 2.7 (Table 2, Figure 2f, green). The wear of the bearing washer was reduced by 93 %  
345 (shaft washer) and 61 % (housing washer), respectively (Table 2, Figure 2h and i, green). The  
346 observed wear reduction was similar to the a-C:H:W and the a-C coatings as well as superior to  
347 MoS<sub>2</sub>. Considering the deposited masses (see discussion in section 3.1) and the higher density of  
348 MXenes as well as MoS<sub>2</sub> compared to DLC, it can be assumed that the total wear volume was also  
349 substantially reduced. This indicates that MXenes are a rather clean ("green") solid lubricant. With  
350 regard to combining an extended service life with smooth operation and low frictional torques, the  
351 more easy-to-shear and less adhering coatings (MXenes, MoS<sub>2</sub>, and the more graphite-like a-C)  
352 seemed to be particularly suitable due to their potential tribo-film formation and transfer to the  
353 counter-bodies. For MoS<sub>2</sub> and GLC, this had previously been reported in literature [14,75–77], but  
354 we were not able to verify the respective transfer to the counter bodies for these coatings after fatal  
355 bearing failure. In case of the MXene coating, some areas of the bearing raceways were exposed  
356 and affected by wear, while other regions were still protected by films of compacted nano-  
357 sheets (Figure 3a). Based upon optical micrographs (Figure 3b and c) and the corresponding Raman  
358 spectra (Figure 3d), which featured typical MXene peaks at about 222, 290, 380 and 600 cm<sup>-1</sup>, it  
359 becomes evident that lubricious material originating from a tribo-layer was transferred to secondary  
360 tribo-contacts of the bearing (particularly the contacts between rolling elements and cage pockets),  
361 thus enhancing the friction and wear performance. This mechanism is schematically illustrated in  
362 Figure 3e. Based upon our previous studies and the available literature, Ti<sub>3</sub>C<sub>2</sub>T<sub>x</sub> nano-sheets have  
363 shown to enable the formation of lubricious tribo-layers consisting of degraded MXenes intermixed  
364 with nanocrystalline/amorphous oxide structures (mostly iron oxide from the substrate with some  
365 titanium oxide) [45]. These beneficial tribo-layers have been demonstrated to extend the coatings'  
366 lifetime, thus notably contributing to their durability and longevity. Regarding the MXenes'  
367 degradation, the thermomechanical and cyclic stress during tribological testing may induce  
368 structural and chemical changes (reduced number of layers, reduced x-y dimensions, increased



369 defect density, and oxidation) [45]. This was also reflected in changed peak intensities and positions  
 370 in the Raman spectrum (Figure 3d) compared to the as-deposited coating (Figure 11). However, the  
 371 Raman signal after the experiment did not indicate excessive oxidation, which also suggests that the  
 372 synthesis process did not substantially result in major oxidation of the as-deposited MXenes.



373

374 **Figure 3.** Optical light micrographs (a) raceway, (b) ball and (c) cage of the run MXene-coated  
 375 bearing as well as (d) averaged Raman spectra. The marks correspond to the positions for Raman  
 376 measurements. (e) Schematic illustration of the underlying mechanisms based upon compacted  
 377 MXene nano-sheets and transfer films acting as solid lubricants between primary (ball/raceway) and  
 378 secondary (ball/cage) rolling bearing contacts.

379 In general, our results indicate that the service life of the MXene-coated bearing was extended by  
 380 30 and 55 % compared to MoS<sub>2</sub> and DLC coating, respectively (Figure 2f). This observation has to  
 381 be assessed against the background of potential influences regarding different morphologies of the  
 382 coatings as well as testing and environmental conditions onto the tribological performance of solid  
 383 lubricants like MoS<sub>2</sub> and DLC [78,79], which, however, equally apply to MXenes [41]. It should be  
 384 emphasized that MoS<sub>2</sub> and DLC have already been explored and optimized for their usage in rolling  
 385 bearings over several decades [80,81]. Our experimental finding that MXenes show a comparable  
 386 or even superior performance underlines their tremendous potential, especially considering the early  
 387 stage of tribological research. More research effort needs to be dedicated towards the deposition of

388 more uniform MXene coatings with improved interfacial and adhesive properties by utilizing spray  
389 coating or electrophoretic deposition [5,45]. However, it should be noted that certain initial  
390 wear can be beneficial to initiate the tribo-film formation as well as the respective transfer to the  
391 counter bodies, which may lead to ultralow wear in secondary contacts of the machine  
392 components [45]. Despite the investigated thrust ball bearings feature several contacts,  
393 including lower-loaded secondary sliding contacts between ball and cage and the higher-  
394 loaded primary rolling-sliding contacts between ball and raceway, basic model tests under  
395 rolling-sliding motion (two-disk tribometer or mini traction machine) are advisable in the future  
396 for an improved understanding of the fundamental mechanisms. This also comprises the study of  
397 the influence of thermal properties with regard to cooling effects as well as the damping of  
398 vibrations. Furthermore, future research work regarding the usage of further MXenes with  
399 different stoichiometry or early transition metals [4,7] as well as tailored surface  
400 functionalization by making use of their richness in available surface terminations will further boost  
their tribological performance [5].

401

#### 402 **4. Conclusions**

403 MXenes have recently shown excellent solid lubrication ability with an enhanced wear performance  
404 due to their weakly bonded multi-layer structure and tribofilm formation with self-lubricating  
405 character, which is of particular interest for dry-running tribo-systems. This contribution  
406 investigated the friction and wear performance of multi-layer  $Ti_3C_2T_x$  coatings applied to rolling  
407 bearings and compared the tribological performance of MXenes with the performance of state-of-  
408 the art solid lubricant coatings including  $MoS_2$ , a-C:H:W, and a-C. It was found that  
409 MXene coatings reduced wear on the bearing washers by up to 94 % relative to uncoated  
410 references, which was comparable to DLC coatings and even superior to  $MoS_2$  coatings. While the  
411 frictional torque of all solid lubricants was similar during steady-state operation, the MXene-  
412 coated bearings extended the average service life by 30 and 55 % compared to  $MoS_2$  and DLC,  
413 respectively. This was traced back to the transfer of lubricious nano-sheets to secondary tribo-  
contacts of the bearing, particularly between rolling elements and cage pockets, which was  
verified by Raman spectroscopy. This

414 contribution demonstrated MXenes' general ability to outperform state-of-the-art solid lubricants  
415 when applied to dry-running machine components such as rolling bearings.

#### 416 **Conflict of Interest**

417 The authors declare that they have no known competing financial interests or personal relationships that  
418 could have appeared to influence the work reported in this manuscript.

419

#### 420 **Acknowledgments**

421 M. Marian, B. Rothhammer, M. Bartz and S. Wartzack greatly acknowledge the continuous support of  
422 Friedrich-Alexander-University Erlangen-Nuremberg (FAU), Germany.

#### 423 **Funding**

424 A. Seynstahl, S. Tremmel, S. Krauß and B. Merle acknowledge the financial support by the German  
425 Research Foundation (DFG) within the priority program SPP 2074 "Fluid-free lubrication systems with high  
426 mechanical loads" (407707942, TR 1043/7-1, ME 4368/7-1). A. Rosenkranz acknowledges the financial  
427 support given by ANID-CONICYT within the project Fondecyt 11180121 and the VID of the University of  
428 Chile in the framework of U-Inicia UI013/2018. A. Rosenkranz and B. Wang acknowledge the financial  
429 support of the Chinese Academy of Sciences President's International Fellowship Initiative (2020VEC0006).

#### 430 **Author Contributions**

431 M. Marian conceived the idea. B. Wang synthesized the  $Ti_3C_2T_x$  nano-sheets. B. Rothhammer and  
432 A. Seynstahl designed and deposited the DLC and  $MoS_2$  coatings. S. Krauß and T. Böhm characterized the  
433 as-deposited coatings by SEM, EDX and Raman spectroscopy. K. Feile and M. Marian carried out the  
434 experiments and analyzed the data. M. Marian and A. Rosenkranz wrote the manuscript. All authors  
435 contributed to the discussion and have reviewed, edited, and approved the final version of the manuscript.

#### 436 **References**

- 437 [1] M. Naguib, V.N. Mochalin, M.W. Barsoum, Y. Gogotsi, 25th anniversary article: MXenes: a new family  
438 of two-dimensional materials, *Adv. Mater. Weinheim.* 26 (2014) 992–1005.  
439 <https://doi.org/10.1002/adma.201304138>.
- 440 [2] B. Anasori, M.R. Lukatskaya, Y. Gogotsi, 2D metal carbides and nitrides (MXenes) for energy storage,  
441 *Nature Reviews Materials* 2 (2017) 16098. <https://doi.org/10.1038/natrevmats.2016.98>.
- 442 [3] M. Naguib, M. Kurtoglu, V. Presser, J. Lu, J. Niu, M. Heon, L. Hultman, Y. Gogotsi, M.W. Barsoum,  
443 Two-dimensional nanocrystals produced by exfoliation of Ti<sub>3</sub>AlC<sub>2</sub>, *Adv. Mater. Weinheim.* 23 (2011)  
444 4248–4253. <https://doi.org/10.1002/adma.201102306>.
- 445 [4] B. Anasori, Y. Gogotsi, 2D Metal Carbides and Nitrides (MXenes): Structure, Properties and  
446 Applications, Springer International Publishing; Imprint: Springer, Cham, 2019.
- 447 [5] B.C. Wyatt, A. Rosenkranz, B. Anasori, 2D MXenes: Tunable Mechanical and Tribological Properties,  
448 *Adv. Mater. Weinheim.* (2021) e2007973. <https://doi.org/10.1002/adma.202007973>.
- 449 [6] T. Hu, M. Hu, Z. Li, H. Zhang, C. Zhang, J. Wang, X. Wang, Interlayer coupling in two-dimensional  
450 titanium carbide MXenes, *Phys. Chem. Chem. Phys.* 18 (2016) 20256–20260.  
451 <https://doi.org/10.1039/C6CP01699E>.
- 452 [7] Y. Gogotsi, B. Anasori, The Rise of MXenes, *ACS Nano* 13 (2019) 8491–8494.  
453 <https://doi.org/10.1021/acsnano.9b06394>.
- 454 [8] D. Zhang, M. Ashton, A. Ostadhossein, A.C.T. van Duin, R.G. Hennig, S.B. Sinnott, Computational  
455 Study of Low Interlayer Friction in Tin+1C<sub>n</sub> (n = 1, 2, and 3) MXene, *ACS Appl. Mater. Interfaces* 9  
456 (2017) 34467–34479. <https://doi.org/10.1021/acsnano.7b09895>.
- 457 [9] C. Donnet, A. Erdemir, Solid Lubricant Coatings: Recent Developments and Future Trends, *Tribol Lett*  
458 17 (2004) 389–397. <https://doi.org/10.1023/B:TRIL.0000044487.32514.1d>.
- 459 [10] C. Donnet, A. Erdemir, Historical developments and new trends in tribological and solid lubricant  
460 coatings, *Surf. Coat. Technol.* 180-181 (2004) 76–84. <https://doi.org/10.1016/j.surfcoat.2003.10.022>.
- 461 [11] T.W. Scharf, S.V. Prasad, Solid lubricants: a review, *J Mater Sci* 48 (2013) 511–531.  
462 <https://doi.org/10.1007/s10853-012-7038-2>.
- 463 [12] S. Rao, M. Sandeep, R. Kumaraswami, A. Shravan, A critical review on solid lubricants, *International*  
464 *Journal of Mechanical Engineering and Technology* 7 (2016) 193–199.
- 465 [13] S.H. Wan, Solid Lubricant: Soft Metal, in: Q.J. Wang, Y.-W. Chung (Eds.), *Encyclopedia of Tribology*,  
466 Springer US, Boston, MA, 2013, pp. 3152–3159.
- 467 [14] M.R. Vazirisereshk, A. Martini, D.A. Strubbe, M.Z. Baykara, Solid Lubrication with MoS<sub>2</sub>: A Review,  
468 *Lubricants* 7 (2019) 57. <https://doi.org/10.3390/lubricants7070057>.
- 469 [15] H.S. Khare, D.L. Burris, The Effects of Environmental Water and Oxygen on the Temperature-  
470 Dependent Friction of Sputtered Molybdenum Disulfide, *Tribol Lett* 52 (2013) 485–493.  
471 <https://doi.org/10.1007/s11249-013-0233-8>.
- 472 [16] B. Vierneusel, T. Schneider, S. Tremmel, S. Wartzack, T. Gradt, Humidity resistant MoS<sub>2</sub> coatings  
473 deposited by unbalanced magnetron sputtering, *Surf. Coat. Technol.* 235 (2013) 97–107.  
474 <https://doi.org/10.1016/j.surfcoat.2013.07.019>.

- 475 [17] A. Mesgarnejad, M.M. Khonsari, On the tribological behavior of MoS<sub>2</sub>-coated thrust ball bearings  
476 operating under oscillating motion, *Wear* 269 (2010) 547–556.  
477 <https://doi.org/10.1016/j.wear.2010.05.010>.
- 478 [18] H. Singh, K.C. Mutyala, H. Mohseni, T.W. Scharf, R.D. Evans, G.L. Doll, Tribological Performance  
479 and Coating Characteristics of Sputter-Deposited Ti-Doped MoS<sub>2</sub> in Rolling and Sliding Contact,  
480 *Tribol. Trans.* 58 (2015) 767–777. <https://doi.org/10.1080/10402004.2015.1015758>.
- 481 [19] D. Berman, A. Erdemir, A.V. Sumant, Graphene: a new emerging lubricant, *Materials Today* 17 (2014)  
482 31–42. <https://doi.org/10.1016/j.mattod.2013.12.003>.
- 483 [20] F. Pape, G. Poll, Investigations on Graphene Platelets as Dry Lubricant and as Grease Additive for  
484 Sliding Contacts and Rolling Bearing Application, *Lubricants* 8 (2020) 3.  
485 <https://doi.org/10.3390/lubricants8010003>.
- 486 [21] C. Donnet, A. Erdemir, *Tribology of Diamond-Like Carbon Films: Fundamentals and Applications*,  
487 Springer, Boston, 2008.
- 488 [22] A.W. Zia, Z. Zhou, L.K.-Y. Li, Structural, mechanical, and tribological characteristics of diamond-like  
489 carbon coatings, in: *Nanomaterials-Based Coatings*, Elsevier, 2019, pp. 171–194.
- 490 [23] J. Kröner, S. Kursawe, Y. Musayev, S. Tremmel, Analysing the Tribological Behaviour of DLC-Coated  
491 Dry-Running Deep Groove Ball Bearings with Regard to the Ball Material, *AMM* 856 (2016) 143–150.  
492 <https://doi.org/10.4028/www.scientific.net/AMM.856.143>.
- 493 [24] J. Kröner, S. Tremmel, S. Wartzack, Untersuchungen an a-C:H:Me-beschichteten Rillenkugellagern  
494 unter Trockenlaufbedingungen, *Tribologie und Schmierungstechnik* 66 (2019) 33–39.  
495 <https://doi.org/10.30419/TuS-2019-0030>.
- 496 [25] A. Vanhulsel, F. Velasco, R. Jacobs, L. Eersels, D. Havermans, E.W. Roberts, I. Sherrington, M.J.  
497 Anderson, L. Gaillard, DLC solid lubricant coatings on ball bearings for space applications, *Tribol. Int.*  
498 40 (2007) 1186–1194. <https://doi.org/10.1016/j.triboint.2006.12.005>.
- 499 [26] A. Rosenkranz, Y. Liu, L. Yang, L. Chen, 2D nano-materials beyond graphene: from synthesis to  
500 tribological studies, *Appl Nanosci* 10 (2020) 3353–3388. <https://doi.org/10.1007/s13204-020-01466-z>.
- 501 [27] M. Malaki, R.S. Varma, Mechanotribological Aspects of MXene-Reinforced Nanocomposites, *Adv.*  
502 *Mater. Weinheim.* 32 (2020) e2003154. <https://doi.org/10.1002/adma.202003154>.
- 503 [28] J. Yang, B. Chen, H. Song, H. Tang, C. Li, Synthesis, characterization, and tribological properties of  
504 two-dimensional Ti<sub>3</sub>C<sub>2</sub>, *Crystal Research and Technology* 49 (2014) 926–932.  
505 <https://doi.org/10.1002/crat.201400268>.
- 506 [29] Y. Liu, X. Zhang, S. Dong, Z. Ye, Y. Wei, Synthesis and tribological property of Ti<sub>3</sub>C<sub>2</sub>TX nanosheets,  
507 *Journal of Materials Science* 52 (2017) 2200–2209. <https://doi.org/10.1007/s10853-016-0509-0>.
- 508 [30] X. Zhang, Y. Guo, Y. Li, Y. Liu, S. Dong, Preparation and tribological properties of potassium titanate-  
509 Ti<sub>3</sub>C<sub>2</sub>T<sub>x</sub> nanocomposites as additives in base oil, *Chinese Chemical Letters* 30 (2019) 502–504.  
510 <https://doi.org/10.1016/j.cclet.2018.07.007>.

- 511 [31] M. Xue, Z. Wang, F. Yuan, X. Zhang, W. Wei, H. Tang, C. Li, Preparation of TiO<sub>2</sub>/Ti<sub>3</sub>C<sub>2</sub>T<sub>x</sub>  
512 hybrid nanocomposites and their tribological properties as base oil lubricant additives, RSC Adv. 7  
513 (2017) 4312–4319. <https://doi.org/10.1039/C6RA27653A>.
- 514 [32] J. Hu, S. Li, J. Zhang, Q. Chang, W. Yu, Y. Zhou, Mechanical properties and frictional resistance of Al  
515 composites reinforced with Ti<sub>3</sub>C<sub>2</sub>T<sub>x</sub> MXene, Chinese Chemical Letters 31 (2020) 996–999.  
516 <https://doi.org/10.1016/j.ccl.2019.09.004>.
- 517 [33] Y.J. Mai, Y.G. Li, S.L. Li, L.Y. Zhang, C.S. Liu, X.H. Jie, Self-lubricating Ti<sub>3</sub>C<sub>2</sub> nanosheets/copper  
518 composite coatings, Journal of Alloys and Compounds 770 (2019) 1–5.  
519 <https://doi.org/10.1016/j.jallcom.2018.08.100>.
- 520 [34] H. Zhang, L. Wang, Q. Chen, P. Li, A. Zhou, X. Cao, Q. Hu, Preparation, mechanical and anti-friction  
521 performance of MXene/polymer composites, Materials & Design 92 (2016) 682–689.  
522 <https://doi.org/10.1016/j.matdes.2015.12.084>.
- 523 [35] H. Zhang, L. Wang, A. Zhou, C. Shen, Y. Dai, F. Liu, J. Chen, P. Li, Q. Hu, Effects of 2-D transition  
524 metal carbide Ti<sub>2</sub>C<sub>T<sub>x</sub></sub> on properties of epoxy composites, RSC Adv. 6 (2016) 87341–87352.  
525 <https://doi.org/10.1039/C6RA14560D>.
- 526 [36] W. Lian, Y. Mai, C. Liu, L. Zhang, S. Li, X. Jie, Two-dimensional Ti<sub>3</sub>C<sub>2</sub> coating as an emerging  
527 protective solid-lubricant for tribology, Ceramics International 44 (2018) 20154–20162.  
528 <https://doi.org/10.1016/j.ceramint.2018.07.309>.
- 529 [37] A. Rosenkranz, P.G. Grützmacher, R. Espinoza, V.M. Fuenzalida, E. Blanco, N. Escalona, F.J. Gracia,  
530 R. Villarroel, L. Guo, R. Kang, F. Mücklich, S. Suarez, Z. Zhang, Multi-layer Ti<sub>3</sub>C<sub>2</sub>T<sub>x</sub>-nanoparticles  
531 (MXenes) as solid lubricants – Role of surface terminations and intercalated water, Appl. Surf. Sci. 494  
532 (2019) 13–21. <https://doi.org/10.1016/j.apsusc.2019.07.171>.
- 533 [38] Y. Guo, X. Zhou, D. Wang, X. Xu, Q. Xu, Nanomechanical Properties of Ti<sub>3</sub>C<sub>2</sub> MXene, Langmuir 35  
534 (2019) 14481–14485. <https://doi.org/10.1021/acs.langmuir.9b02619>.
- 535 [39] X. Zhou, Y. Guo, D. Wang, Q. Xu, Nano friction and adhesion properties on Ti<sub>3</sub>C<sub>2</sub> and Nb<sub>2</sub>C MXene  
536 studied by AFM, Tribol. Int. 153 (2021) 106646. <https://doi.org/10.1016/j.triboint.2020.106646>.
- 537 [40] A. Rodriguez, M.S. Jaman, O. Acikgoz, B. Wang, J. Yu, P.G. Grützmacher, A. Rosenkranz, M.Z.  
538 Baykara, The potential of Ti<sub>3</sub>C<sub>2</sub>T<sub>x</sub> nano-sheets (MXenes) for nanoscale solid lubrication revealed by  
539 friction force microscopy, Appl. Surf. Sci. 535 (2021) 147664.  
540 <https://doi.org/10.1016/j.apsusc.2020.147664>.
- 541 [41] M. Marian, G.C. Song, B. Wang, V.M. Fuenzalida, S. Krauß, B. Merle, S. Tregmel, S. Wartzack, J.  
542 Yu, A. Rosenkranz, Effective usage of 2D MXene nanosheets as solid lubricant – Influence of contact  
543 pressure and relative humidity, Appl. Surf. Sci. 531 (2020) 147311.  
544 <https://doi.org/10.1016/j.apsusc.2020.147311>.
- 545 [42] X. Yin, J. Jin, X. Chen, A. Rosenkranz, J. Luo, Ultra-Wear-Resistant MXene-Based Composite Coating  
546 via in Situ Formed Nanostructured Tribofilm, ACS Appl. Mater. Interfaces 11 (2019) 32569–32576.  
547 <https://doi.org/10.1021/acsami.9b11449>.

- 548 [43] X. Yin, J. Jin, X. Chen, A. Rosenkranz, J. Luo, Interfacial Nanostructure of 2D Ti<sub>3</sub>C<sub>2</sub>/Graphene QDs  
549 Hybrid Multicoating for Ultralow Wear, *Adv. Eng. Mater.* (2020).  
550 <https://doi.org/10.1002/adem.201901369>.
- 551 [44] H. Yan, L. Zhang, H. Li, X. Fan, M. Zhu, Towards high-performance additive of Ti<sub>3</sub>C<sub>2</sub>/graphene  
552 hybrid with a novel wrapping structure in epoxy coating, *Carbon* 157 (2020) 217–233.  
553 <https://doi.org/10.1016/j.carbon.2019.10.034>.
- 554 [45] P.G. Grützmacher, S. Suarez, A. Tolosa, C. Gachot, G. Song, B. Wang, V. Presser, F. Mücklich, B.  
555 Anasori, A. Rosenkranz, Superior Wear-Resistance of Ti<sub>3</sub>C<sub>2</sub>Tx Multilayer Coatings, *ACS Nano*  
556 (2021). <https://doi.org/10.1021/acsnano.1c01555>.
- 557 [46] H. Singh, K.C. Mutyala, R.D. Evans, G.L. Doll, An investigation of material and tribological properties  
558 of Sb<sub>2</sub>O<sub>3</sub>/Au-doped MoS<sub>2</sub> solid lubricant films under sliding and rolling contact in different  
559 environments, *Surf. Coat. Technol.* 284 (2015) 281–289. <https://doi.org/10.1016/j.surfcoat.2015.05.049>.
- 560 [47] M. Marian, S. Tremmel, S. Wartzack, G. Song, B. Wang, J. Yu, A. Rosenkranz, MXene nanosheets as  
561 an emerging solid lubricant for machine elements – Towards increased energy efficiency and service  
562 life, *Appl. Surf. Sci.* 523 (2020) 1–8. <https://doi.org/10.1016/j.apsusc.2020.146503>.
- 563 [48] ISO, 104:2015-09 Rolling bearings - Thrust bearings - Boundary dimensions, general plan.
- 564 [49] X. Shi, T.W. Liskiewicz, B.D. Beake, Z. Sun, J. Chen, Fretting wear behavior of graphite-like carbon  
565 films with bias-graded deposition, *Appl. Surf. Sci.* 494 (2019) 929–940.  
566 <https://doi.org/10.1016/j.apsusc.2019.07.265>.
- 567 [50] X. Shi, T.W. Liskiewicz, B.D. Beake, J. Chen, C. Wang, Tribological performance of graphite-like  
568 carbon films with varied thickness, *Tribol. Int.* 149 (2020) 105586.  
569 <https://doi.org/10.1016/j.triboint.2019.01.045>.
- 570 [51] J. Kröner, S. Tremmel, S. Kursawe, Y. Musayev, T. Hosenfeldt, S. Wartzack, GreenBearings – Friction  
571 Behaviour of DLC-Coated Dry Running Deep Groove Ball Bearings, *AMM* 805 (2015) 147–153.  
572 <https://doi.org/10.4028/www.scientific.net/AMM.805.147>.
- 573 [52] A. Seynstahl, S. Krauß, E. Bitzek, B. Meyer, B. Merle, S. Tremmel, Microstructure, Mechanical  
574 Properties and Tribological Behavior of Magnetron-Sputtered MoS<sub>2</sub> Solid Lubricant Coatings  
575 Deposited under Industrial Conditions, *Coatings* 11 (2021) 455.  
576 <https://doi.org/10.3390/coatings11040455>.
- 577 [53] B. Vierneusel, L. Benker, S. Tremmel, M. Göken, B. Merle, Isolating the effect of residual stresses on  
578 coating wear by a mechanical stress relaxation technique, *International Conference on Metallurgical*  
579 *Coatings*, San Diego, 1989 638 (2017) 159–166. <https://doi.org/10.1016/j.tsf.2017.06.016>.
- 580 [54] E.I. Preiß, B. Merle, Y. Xiao, F. Gannott, J.P. Liebig, J.M. Wheeler, M. Göken, Applicability of  
581 focused Ion beam (FIB) milling with gallium, neon, and xenon to the fracture toughness  
582 characterization of gold thin films, *J. Mater. Res.* (2021). <https://doi.org/10.1557/s43578-020-00045-w>.
- 583 [55] B. Rothhammer, K. Neusser, M. Marian, M. Bartz, S. Krauß, T. Böhm, S. Thiele, B. Merle, R. Detsch, S.  
584 Wartzack, Amorphous Carbon Coatings for Total Knee Replacements-Part I: Deposition,

- 585 Cytocompatibility, Chemical and Mechanical Properties, *Polymers* 13 (2021).  
586 <https://doi.org/10.3390/polym13121952>.
- 587 [56] A.C. Ferrari, J. Robertson, Raman spectroscopy of amorphous, nanostructured, diamond-like carbon,  
588 and nanodiamond, *Philos. Trans. A Math. Phys. Eng. Sci.* 362 (2004) 2477–2512.  
589 <https://doi.org/10.1098/rsta.2004.1452>.
- 590 [57] W.G. Cui, Q.B. Lai, L. Zhang, F.M. Wang, Quantitative measurements of sp<sup>3</sup> content in DLC films  
591 with Raman spectroscopy, *Surf. Coat. Technol.* 205 (2010) 1995–1999.  
592 <https://doi.org/10.1016/j.surfcoat.2010.08.093>.
- 593 [58] F.C. Tai, S.C. Lee, C.H. Wei, S.L. Tyan, Correlation between  $I_D/I_G$  Ratio from Visible Raman Spectra  
594 and sp<sup>2</sup>/sp<sup>3</sup> Ratio from XPS Spectra of Annealed Hydrogenated DLC Film, *Mater. Trans.* 47 (2006)  
595 1847–1852. <https://doi.org/10.2320/matertrans.47.1847>.
- 596 [59] Y. Wang, H. Li, L. Ji, F. Zhao, Q. Kong, Y. Wang, X. Liu, W. Quan, H. Zhou, J. Chen, Microstructure,  
597 mechanical and tribological properties of graphite-like amorphous carbon films prepared by unbalanced  
598 magnetron sputtering, *Surf. Coat. Technol.* 205 (2011) 3058–3065.  
599 <https://doi.org/10.1016/j.surfcoat.2010.11.019>.
- 600 [60] D.N. Khaemba, A. Neville, A. Morina, A methodology for Raman characterisation of MoDTC  
601 tribofilms and its application in investigating the influence of surface chemistry on friction performance  
602 of MoDTC lubricants, *Tribol Lett* 59 (2015). <https://doi.org/10.1007/s11249-015-0566-6>.
- 603 [61] T.J. Wieting, Long-wavelength lattice vibrations of MoS<sub>2</sub> and GaSe, *Solid State Communications* 12  
604 (1973) 931–935. [https://doi.org/10.1016/0038-1098\(73\)90111-7](https://doi.org/10.1016/0038-1098(73)90111-7).
- 605 [62] B.C. Windom, W.G. Sawyer, D.W. Hahn, A Raman Spectroscopic Study of MoS<sub>2</sub> and MoO<sub>3</sub>:  
606 Applications to Tribological Systems, *Tribol Lett* 42 (2011) 301–310. <https://doi.org/10.1007/s11249-011-9774-x>.
- 608 [63] S. Domínguez-Meister, T.C. Rojas, M. Brizuela, J.C. Sánchez-López, Solid lubricant behavior of MoS<sub>2</sub>  
609 and WSe<sub>2</sub>-based nanocomposite coatings, *Sci. Technol. Adv. Mater.* 18 (2017) 122–133.  
610 <https://doi.org/10.1080/14686996.2016.1275784>.
- 611 [64] J.J. Hu, R. Wheeler, J.S. Zabinski, P.A. Shade, A. Shiveley, A.A. Voevodin, Transmission Electron  
612 Microscopy Analysis of Mo–W–S–Se Film Sliding Contact Obtained by Using Focused Ion Beam  
613 Microscope and In Situ Microtribometer, *Tribol Lett* 32 (2008) 49–57. <https://doi.org/10.1007/s11249-008-9360-z>.
- 615 [65] J.M. Chen, C.S. Wang, Second order Raman spectrum of MoS<sub>2</sub>, *Solid State Communications* 14 (1974)  
616 857–860. [https://doi.org/10.1016/0038-1098\(74\)90150-1](https://doi.org/10.1016/0038-1098(74)90150-1).
- 617 [66] G.L. Frey, R. Tenne, M.J. Matthews, M.S. Dresselhaus, G. Dresselhaus, Raman and resonance Raman  
618 investigation of MoS<sub>2</sub> nanoparticles, *Phys. Rev. B* 60 (1999) 2883–2892.  
619 <https://doi.org/10.1103/PhysRevB.60.2883>.
- 620 [67] M. Hu, T. Hu, Z. Li, Y. Yang, R. Cheng, J. Yang, C. Cui, X. Wang, Surface Functional Groups and  
621 Interlayer Water Determine the Electrochemical Capacitance of Ti<sub>3</sub>C<sub>2</sub> T<sub>x</sub> MXene, *ACS Nano* 12  
622 (2018) 3578–3586. <https://doi.org/10.1021/acsnano.8b00676>.



- 623 [68] T. Hu, J. Wang, H. Zhang, Z. Li, M. Hu, X. Wang, Vibrational properties of Ti<sub>3</sub>C<sub>2</sub> and Ti<sub>3</sub>C<sub>2</sub>T<sub>2</sub> (T =  
624 O, F, OH) monosheets by first-principles calculations: a comparative study, *Phys. Chem. Chem. Phys.*  
625 17 (2015) 9997–10003. <https://doi.org/10.1039/C4CP05666C>.
- 626 [69] X. Zhang, Y. Liu, S. Dong, Z. Ye, Y. Guo, One-step hydrothermal synthesis of a TiO<sub>2</sub>-Ti<sub>3</sub>C<sub>2</sub>T<sub>x</sub>  
627 nanocomposite with small sized TiO<sub>2</sub> nanoparticles, *Ceramics International* 43 (2017) 11065–11070.  
628 <https://doi.org/10.1016/j.ceramint.2017.05.151>.
- 629 [70] A. Sarycheva, Y. Gogotsi, Raman Spectroscopy Analysis of the Structure and Surface Chemistry of Ti  
630 <sub>3</sub> C <sub>2</sub> T <sub>x</sub> MXene, *Chem. Mater.* 32 (2020) 3480–3488.  
631 <https://doi.org/10.1021/acs.chemmater.0c00359>.
- 632 [71] V. Buck, Structure and density of sputtered MoS<sub>2</sub>-films, *Vacuum* 36 (1986) 89–94.  
633 [https://doi.org/10.1016/0042-207X\(86\)90277-0](https://doi.org/10.1016/0042-207X(86)90277-0).
- 634 [72] A. LiBassi, A.C. Ferrari, V. Stolojan, B.K. Tanner, J. Robertson, L.M. Brown, Density, sp<sup>3</sup> content  
635 and internal layering of DLC films by X-ray reflectivity and electron energy loss spectroscopy,  
636 *Diamond and Related Materials* 9 (2000) 771–776. [https://doi.org/10.1016/S0925-9635\(99\)00233-2](https://doi.org/10.1016/S0925-9635(99)00233-2).
- 637 [73] D.K. Avasthi, D. Kabiraj, Jaipal, G.K. Mehta, H.C. Barshilia, S. Sah, B.R. Mehta, v.d. Vankar, Study of  
638 hydrogen in DLC film by ERDA with <sup>58</sup>Ni ions, *Vacuum* 46 (1995) 633–636.  
639 [https://doi.org/10.1016/0042-207X\(95\)00004-6](https://doi.org/10.1016/0042-207X(95)00004-6).
- 640 [74] B. Vierneusel, Verschleiß- und feuchteresistente MoS<sub>2</sub>-Festschmierstoffschichten für den Gleit- und  
641 Wälzkontakt: Reihe 1, Konstruktionstechnik, Maschinenelemente, Nr. 440, Fortschritt-Berichte VDI,  
642 Düsseldorf, 2017.
- 643 [75] Y. Wang, J. Li, L. Shan, J. Chen, Q. Xue, Tribological performances of the graphite-like carbon films  
644 deposited with different target powers in ambient air and distilled water, *Tribol. Int.* 73 (2014) 17–24.  
645 <https://doi.org/10.1016/j.triboint.2013.12.022>.
- 646 [76] S.K. Field, M. Jarratt, D.G. Teer, Tribological properties of graphite-like and diamond-like carbon  
647 coatings, *Tribol. Int.* 37 (2004) 949–956. <https://doi.org/10.1016/j.triboint.2004.07.012>.
- 648 [77] S.-C. Shi, J.-Y. Wu, Y.-Q. Peng, Transfer layer formation in MoS<sub>2</sub>/hydroxypropyl methylcellulose  
649 composite, *Wear* 408-409 (2018) 208–213. <https://doi.org/10.1016/j.wear.2018.05.019>.
- 650 [78] Z. Chen, X. He, C. Xiao, S. Kim, Effect of Humidity on Friction and Wear—A Critical Review,  
651 *Lubricants* 6 (2018) 74. <https://doi.org/10.3390/lubricants6030074>.
- 652 [79] L. Wang, L. Bai, Z. Lu, G. Zhang, Z. Wu, Influence of Load on the Tribological Behavior of a-C Films:  
653 Experiment and Calculation Coupling, *Tribol Lett* 52 (2013) 469–475. <https://doi.org/10.1007/s11249-013-0230-y>.
- 654 [80] R. Christy, Sputtered MoS<sub>2</sub> lubricant coating improvements, *Thin Solid Films* 73 (1980) 299–307.  
655 [https://doi.org/10.1016/0040-6090\(80\)90493-9](https://doi.org/10.1016/0040-6090(80)90493-9).
- 656 [81] M. Nishimura, M. Suzuki, Solid-lubricated ball bearings for use in a vacuum — state-of-the-art, *Tribol.*  
657 *Int.* 32 (1999) 637–647. [https://doi.org/10.1016/S0301-679X\(99\)00089-4](https://doi.org/10.1016/S0301-679X(99)00089-4).
- 658